

Predicting sit-to-stand adaptations due to muscle strength deficits and assistance trajectories to complement them

Vinay Kumar^{1,*}, Takahide Yoshiike², and Tomohiro Shibata^{1,*}

¹Department of Human Intelligence Systems, Graduate School of Life Science and Systems Engineering, Kyushu Institute of Technology, Kitakyushu, Japan

²Honda R&D Co., Ltd., Saitama, Japan

Correspondence*:

Vinay Kumar
vinaym815@gmail.com

Tomohiro Shibata

tom@brain.kyutech.ac.jp

2 ABSTRACT

3 Sit-to-stand (STS) transition is the most bio-mechanically challenging task necessary for
 4 performing activities of daily life. With muscle strength being the most dominant, many co-
 5 occurring factors influence how individuals perform STS transition. This study investigates muscle
 6 strength deficits for the STS adaptations they cause and how they might lead to unsuccessful
 7 STS transition. It also presents external assistance trajectories that can complement strength
 8 deficits for successful STS transition. Towards these aims, this study uses the STS trajectories
 9 generated using single shooting optimization as the presence of many co-occurring factors makes
 10 it complex to establish cause-effect relationships using experiments. The optimization tuned the
 11 open-loop excitation trajectories of muscles and external assistance. The planar musculoskeletal
 12 model used in this study features three degrees of freedom and eight hill-type muscles. The
 13 muscle strength deficits were increased in steps of 20%, and the STS trajectories were generated
 14 for each musculoskeletal model. The optimization could generate successful STS transition for
 15 the 0%, 20%, and 40% strength deficit models. We report the common muscle activation patterns
 16 among these STS trajectories and contrast them against those observed experimentally in the
 17 literature. Then these trajectories are compared to each other to observe the STS adaptations
 18 caused by strength deficits. Primarily the motion becomes less explosive with increased STS
 19 durations and lower peak muscle forces and center of mass velocities. Also, the hamstring muscle
 20 activation reduces, which relieves the antagonistic vastus muscles but stresses the agnostic
 21 gluteus muscle. Subsequently, the 60% strength deficit model was aided using ideal torques
 22 actuators at the hip, knee, and ankle joints and used to track the successful STS trajectory of
 23 the 40% strength deficit model with OpenSim CMC tool. The torque actuators aided significantly
 24 only when the muscles could not generate sufficient forces to track the motion. The results from
 25 this motion tracking are used to propose the vastus muscle weakness as the principal reason
 26 behind unsuccessful STS transition. Finally, the STS trajectory generated for the 60% strength
 27 deficit model externally assisted at the torso is presented. The generated trajectory features
 28 lower muscle forces and the utilization of external assistance as and when needed. We hope the
 29 results of this will help plan intervention and design novel STS assistance devices.

30 **Keywords:** Sit-To-Stand, Musculoskeletal Model, Strength Deficit, Single Shooting Optimization, Open Loop Controller, Assist-A-
 31 Needed

1 INTRODUCTION

Sit-to-stand (STS) transition is a precursor to walking, hence critical for performing daily life activities and an independent lifestyle. A successful STS transition requires more effort by the hip and knee extensors than walking or climbing stairs (Hughes et al., 1996). Consequently, it is the first mobility task with which most people develop problems. This study identifies the STS adaptations caused by muscle strength deficits, investigates how strength deficits may lead to unsuccessful STS transition, and finally, presents the external assistance trajectories that can complement muscle strength deficits for successful STS transition.

Muscle strength deficits are one of the primary causes of unsuccessful STS and have consequently attracted many studies. Most of these studies primarily use inverse dynamical analysis of the experimentally recorded data (Hughes et al., 1996; Schenkman et al., 1996; Gross et al., 1998; Meijer et al., 2009; Caruthers et al., 2020). However, many co-occurring factors influence how an individual performs STS (Lord et al., 2002; Janssen et al., 2002). This co-occurrence complicates the extension of correlational findings from experiments to cause-effect relationships. Also, the inverse dynamical analysis does not allow the actuators to shape, modify or adapt the experimentally recorded data. This non-adaptation might be especially problematic if the data was recorded for subjects without strength deficits (Caruthers et al., 2020). Therefore, this study uses the STS trajectories generated using single shooting optimization towards its aims. The optimization tuned the open-loop excitation trajectories of muscles and external assistance. These excitation trajectories were used to run forward simulations during optimization, thus enabling the muscle strength deficits to shape the generated STS trajectories.

In literature, studies that have used optimization to generate STS transitions have often utilized human models with independent torque actuated joints (Yoshioka et al., 2007; Sadeghi et al., 2013; Mombaur and Hoang, 2017; Geravand et al., 2017). The hamstrings and the rectus femoris are two biarticular muscles that play an essential role in the STS transition. Their biarticularity couples the torques produced at the hip and knee joints. This coupling should not be ignored, especially when designing STS assistance devices, as it may lead to a device that over actuates one of these muscles, leading to muscle contracture and eventually lower back issues. The coupling is also crucial in the investigation of strength deficits for STS adaptations and STS failure. Therefore, this study uses a planar musculoskeletal model featuring three degrees of freedom and eight hill-type muscles instead of a torque actuated human model. The OpenSim API (Delp et al., 2007) was used to formulate the system's equation of motion and their forward integration.

To the best of our knowledge, only three studies in the past, i.e., Pandy et al. (1995); Bobbert et al. (2016), and Yokota et al. (2016), have utilized musculoskeletal models with optimization to generate STS trajectories. Pandy et al. (1995) presented a cost function that generates STS trajectories with similar muscle activations to those of experiments. Bobbert et al. (2016) and Yokota et al. (2016) searched for trajectories that reduced loads on the muscles and the knee joint. Bobbert et al. (2016) also made observations regarding the STS adaptations caused by muscle weakness. This study, like Bobbert et al. (2016), also makes observations about STS adaptations caused by strength deficits. However, the parts of STS failure investigation and the generation of externally assisted STS trajectory are novel. Both Pandy et al. (1995) and Yokota et al. (2016) used open-loop single shooting trajectory optimization while Bobbert et al. (2016) used direct collocation. We used open-loop single shooting trajectory optimization for its straightforward implementation and effortless extension to incorporate closed-loop controllers in future works. Pandy et al. (1995) used sequential gradient programming with the gradients obtained using finite differences for optimization while Yokota et al. (2016) used a multi-objective genetic algorithm for optimization and

73 then manually selected the final solution. We have used the active covariance matrix adaptation evolution
74 strategy (Arnold and Hansen, 2010), or aCMA-ES in short, as the optimizer. It is a stochastic gradient-free
75 optimization algorithm and was selected for its enhanced robustness to the locally optimal solution than
76 the gradient-based methods.

77 We increased strength deficits in steps of 20% and generated STS trajectories for each musculoskeletal
78 model. The muscle strength deficits were introduced by scaling the maximum isometric force of all the
79 muscles simultaneously. The optimization could generate successful STS trajectories for 0%, 20%, and 40%
80 strength deficit models. These STS trajectories are used to observe the common muscle activation patterns
81 and the adaptations caused by muscle strength deficits. Subsequently, the 60% strength deficit model was
82 complemented with ideal torque actuators at the hip, knee, and ankle joints. Then, this model was used
83 with the OpenSim CMC tool (Delp et al., 2007) to track the successful STS trajectory of 40% strength.
84 The ideal torque actuators produced torques only when the muscles could not generate sufficient force to
85 track the motion. This motion tracking is used to propose an explanation for the failure of optimization to
86 generate successful STS trajectories using the unaided 60% strength deficit model.

87 When provided in an assist-as-needed manner, physical assistance can help maintain or recover lower
88 extremity strength. Mombaur and Hoang (2017) and Geravand et al. (2017) have generated physical
89 assistance trajectories to support part of the user's weight during the STS and squat-to-stand motions.
90 However, both of them use torque-actuated human models, and we have already discussed their drawbacks.
91 Thus the STS trajectory generated using the externally assisted 60% strength deficit model is reported. The
92 musculoskeletal model was externally assisted at the torso.

93 It is not easy to identify and detail all of the parameters that influence the generated STS trajectories. For
94 example, Bobbert et al. (2016), and Yokota et al. (2016) does not contain information about the initial
95 guesses to the optimization algorithm, while Pandy et al. (1995) does not include information about the
96 mechanical limits used to restrict the motion to the physiologically plausible range. Thus we have made
97 all the source code and results from this study public at <https://github.com/ShibataLab/STS>.
98 We hope the results of this study will help plan intervention and design novel STS assistance devices that
99 operate in an assist-as-needed manner.

100 The rest of the manuscript is structured as follows. In section 2, we provide details of the musculoskeletal
101 model used in this study. Section 3 gives an overview of the optimization framework, the cost function, and
102 the motion-tracking setup. Section 4 details the common muscle activation patterns among the unassisted
103 STS trajectories, observes the adaptations caused by strength deficits, describes the probable reason for
104 unsuccessful STS transition, and presents the externally assisted STS trajectories. Section 5 concludes this
105 study with a summary of the results, the identified shortcomings, and future research directions.

2 MUSCULOSKELETAL MODEL

106 This study's musculoskeletal model, shown in Figure 1, is a simplified version of the LaiArnold2017 model
107 (Lai et al., 2017). The source model reflects an average-sized adult male of mass 75 kg and height 170 cm.
108 The simplified model is two-dimensional with eight hill-type muscles and three degrees of freedom. The
109 simplifications were needed to make the optimization problem computationally tractable. The following
110 paragraphs detail some of these simplifications.

111 From the source model, the left leg was removed while the mass and inertia of the right foot were doubled..
112 The right foot was fixed to the ground using a weld joint. Then the degrees of freedom corresponding to the
113 sagittal plane motion of the ankle, knee, and the hip joints were added (Figure 1 **B**). The masses of arms,

114 forearms, and hands were lumped to the torso's center of mass (COM). The 0° angle of the hip, knee, and
 115 ankle joints corresponds model standing upright. From this posture, positive angles correspond to ankle
 116 dorsiflexion, knee flexion, and hip flexion; and negative angles correspond to the opposite.

117 The lower extremity muscles with similar functions from the source model were combined to single
 118 muscle-tendon units as done to Ong et al. (2019). The maximum isometric strengths of the right leg
 119 muscles were doubled to account for the missing left leg muscles. Figure 1 shows the eight hill-type
 120 muscles included in the model, i.e., gluteus maximus, hamstrings, iliopsoas, rectus femoris, vastus,
 121 gastrocnemius, soleus, and tibialis anterior. Table 1 lists the acronyms and maximum isometric strength
 122 used for these muscles in this study. We obtained models with different strength deficits by simultaneously
 123 scaling the maximum isometric strengths of these muscles.

124 The chair-body contact interactions were modeled using a kinematic constraint between the femur and the
 125 chair. The kinematic constraint was disabled during simulation when the vertical reaction forces required
 126 to maintain it turned non-compressive. The model has nonlinear torsional springs representing ligaments at
 127 hip, knee, and ankle joints to limit the motion to a physiologically plausible range. They generate torques
 128 when the hip joint flex beyond 120° or extends below 30° , or the knee joint flex beyond 140° or extend
 129 beyond 0° , or the ankle dorsiflex beyond 30° or plantarflex beyond 40° .

130 The external assistance was introduced at the torso's COM to complement the muscle strength deficits.
 131 The rationale behind introducing it at the torso is explained in subsection 4.3. The external assistance
 132 was modeled using two independent point forces acting in the vertical and horizontal directions. Their
 133 respective magnitudes were limited to the $0\text{-}400\text{ N}$ range. The excitation signals were passed through
 134 first-order activation dynamics before being sent to point forces for actuation. The first-order activation
 135 dynamics is the same as that of the hill-type muscle model (Millard, 1999) and had a time constant of 0.1
 136 sec. It made the assistance trajectories smoother and thus helped the optimization algorithm.

3 OPTIMIZATION FRAMEWORK

137 An overview of the single shooting optimization framework used in this study is shown in Figure 2. The
 138 optimization framework uses aCMA-ES algorithm (Arnold and Hansen, 2010) to optimize the values of
 139 decision variables. aCMA-ES is a stochastic gradient-free optimization algorithm that adapts a Gaussian
 140 distribution towards low energy regions. At each generation, aCMA-ES samples a population of candidate
 141 solutions from the Gaussian distribution. Subsequently, all candidates are evaluated for cost values by
 142 running forward simulations. aCMA-ES then adapts the Gaussian distribution based on the cost values and
 143 moves on to the next generation.

144 The excitation trajectories of the muscles and external assistance are discretized using piecewise linear
 145 functions. The values node points obtained from this discretization are the decision variables of our
 146 optimization problem. The time difference between the consecutive node points (dt) had a fixed value of
 147 0.1 sec. The upper limit of simulation duration was 1.6 sec. The musculoskeletal model has 8 hill-type
 148 muscles and 2 point force representation of external assistance. Thus, the optimization problem had 136
 149 decision variables when generating unaided STS trajectories and 170 decision variables when generating
 150 assisted STS trajectories. The excitation values corresponding to the model sitting in the chair were used
 151 as the initial guess to the aCMA-ES. A standard deviation of 0.3 was used as the initial guess for each
 152 decision variable to the optimization algorithm. A population size of 90 was used for each generation. The
 153 optimization algorithm was stopped if the number of generations exceeded 7000 or if the cost function
 154 improved less than 0.5 in the last 250 generations. We used the *libcmaes* library (CMA-ES, 2013) for the
 155 aCMA-ES algorithm. The following subsections include details of the simulation setup and the cost function

156 used with the optimization framework and a summary of the OpenSim CMC tool-based motion-tracking
 157 setup used to analyze results.

158 **3.1 Simulation Setup**

159 The STS simulation is divided into two phases. During the first phase, the kinematic constraint between
 160 the femur and chair plane, representing the chair-body contact interactions, was active, while during the
 161 second phase, it was not. The kinematic constraint was disabled during simulation when the vertical
 162 reaction forces required to maintain it turned non-compressive. Once disabled, the kinematic constraint
 163 could not be re-engaged, i.e., the simulation could only transition from the first phase to the second one
 164 and not vice-versa. The two-phase simulation division prevented optimization from getting stuck into
 165 local optima with multiple chair rises. At the beginning of the simulation, the muscle states were set
 166 by equilibrating the muscle and tendon forces with the muscle activations prescribed by the excitation
 167 trajectories. The upper limit of simulation duration was fixed to 1.6 seconds, as this is approximately the
 168 time a young adult takes to stand up. The simulation was terminated before 1.6 sec if the model approached
 169 the condition of being upright represented in Equation 1.

$$|\theta_{hip}| + |\theta_{knee}| + |\theta_{ankle}| \leq 10^\circ \quad (1)$$

170 **3.2 Cost Function**

171 The cost function which we selected to engender STS transition is a linear combination of ten different
 172 terms and can be expressed as follows:

$$\phi_{total} = \sum_{i=1}^{10} w_i C_i \quad (2)$$

173 where w_i is the relative weight of i^{th} cost term, i.e., C_i . The w_i values were determined heuristically and
 174 are listed in Table 3. The mathematical expressions for the ten cost terms are given in eqs. 3 - 13. Please
 175 refer to Table 2 for the list of symbols used in these equations.

$$C_1 = \int_{t_0}^{t_f} \exp(t|\tau_{boundary}) [y_{com}(t_0) - y_{com}(t)] dt \quad (3)$$

$$C_2 = \int_{t_0}^{t_f} \exp(t|\tau_{boundary}) |x_{talus}(t_0) - x_{com}(t)| dt \quad (4)$$

$$C_3 = \int_{t_0}^{t_f} \exp(t|\tau_{chair}) F_{chair,y}(t) dt \quad (5)$$

$$C_4 = \sqrt{\frac{\sum_m \int_{t_0}^{t_f} a_m(t)^2 dt}{\sum m}} \quad (6)$$

$$C_5 = \sqrt{\frac{\sum_m \int_{t_0}^{t_f} \dot{a}_m(t)^2 dt}{\sum m}} \quad (7)$$

$$C_6 = \int_{t_0}^{t_f} \|F_{Assist}(t)\| dt \quad (8)$$

$$C_7 = \sum_n \int_{t_0}^{t_f} |T_{n,limit}(t)| dt \quad (9)$$

$$C_8 = \int_{t_0}^{t_f} \left(\text{bool}(|F_{feet,x}(t)| > \mu|F_{feet,y}(t)|) \times (|F_{feet,x}(t)| - \mu|F_{feet,y}(t)|) + \text{bool}(|F_{chair,x}(t)| > \mu|F_{chair,y}(t)|) \times (|F_{chair,x}(t)| - \mu|F_{chair,y}(t)|) \right) dt \quad (10)$$

$$C_9 = \int_{t_0}^{t_f} |ZMP_x(t) - x_{talus}(t_0)| dt \quad (11)$$

$$C_{10} = \int_{t_0}^{t_f} -\left(\text{bool}(F_{heel,y}(t) < 0) \times F_{heel,y}(t) + \text{bool}(F_{toe,y}(t) < 0) \times F_{toe,y}(t) \right) dt \quad (12)$$

$$\exp(t|\tau) = \frac{e^{t/\tau}}{\tau[e^{t_f/\tau} - 1]} \quad (13)$$

176 Costs C_1 and C_2 leads the optimization to standing posture. Cost C_3 encourages the transition of
 177 simulation from the first phase to the second. Cost C_4 corresponds to control effort exerted by the muscles
 178 during STS. Cost C_5 ensures that the muscles are activated or deactivated smoothly. Cost C_6 corresponds
 179 to external assistance effort. It was not computed when generating unassisted STS trajectories. Cost C_7
 180 penalizes hyper-flexion and hyper-extension of joints. Cost C_8 penalizes contact forces that would lead to
 181 slip if the bodies were not constrained. Cost C_9 penalizes feet contact forces that would lead to tipping
 182 over the toes or heel. Cost C_{10} penalizes feet contact forces that are non-compressive.

183 Costs C_1 to C_3 use an exponential scaling function, i.e., $\exp()$, expressed in Equation 13. As shown in
 184 Figure 3, the $\exp()$ function gives higher weightage to values observed later in the simulation. Its behavior
 185 is defined entirely by the time constant τ . We used the value of $t_f/24$, also referred to as $\tau_{boundary}$, for the
 186 time constants of terms C_1 and C_2 , and of $t_f/3$, also referred to as τ_{chair} , for the cost term C_3 . Figure 3
 187 shows the graphs of $\exp(t|\tau_{boundary})$ and $\exp(t|\tau_{chair})$ for $t_f = 1.6sec$. The area under the $\exp()$ curve
 188 between 0 to t_f is equal to one. The $\exp()$ function spreads the rewards over a longer duration and makes it
 189 easier for the optimization framework to obtain rewards.

190 The ten cost terms can be divided into three categories. The first category leads the optimization to
 191 standing posture and consists of costs C_1 to C_3 . The second category penalizes the effort exerted and
 192 consists of costs C_4 to C_6 . Costs C_7 to C_{10} belong to the third category representing the constraints the
 193 optimized trajectory should respect. Using an optimization framework that supports non-linear trajectory
 194 constraints, like direct collocation, would have required only the costs from the second category. All
 195 the remaining terms would have been modeled as non-linear trajectory constraints in such a framework.
 196 However, due to its simplicity and ease of future extension to incorporate feedback control loops, we
 197 decided to use the single shooting optimization framework.

198 3.3 Motion Tracking Setup

199 We used the OpenSim CMC tool (Thelen and Anderson, 2006) for motion tracking. The CMC tool
 200 computes the actuator excitation levels at user-specified time intervals that will drive the generalized
 201 coordinates (\vec{q}) of the musculoskeletal model towards a desired kinematic trajectory (\vec{q}_{exp}) in the presence

202 of external forces. At any given time t , the CMC tool first computes the desired acceleration $\ddot{\vec{q}}^*$ using the
 203 following proportional derivative control law:

$$\ddot{\vec{q}}^*(t + T) = \ddot{\vec{q}}_{\text{exp}}(t + T) + \vec{k}_v [\dot{\vec{q}}_{\text{exp}}(t) - \dot{\vec{q}}(t)] + \vec{k}_p [\vec{q}_{\text{exp}}(t) - \vec{q}(t)] \quad (14)$$

204 where, \vec{k}_v and \vec{k}_p are the feedback gains on the velocity and position errors, respectively. Since the
 205 forces that muscles apply cannot change instantaneously, the desired accelerations are computed some
 206 small-time T in the future. Then, CMC tool uses static optimization to distribute the load across synergistic
 207 actuators using static optimization. CMC tool offers two formulations for static optimization referred to as
 208 slow target and fast target. We used the fast target formulation. It minimizes the sum of squared controls
 209 augmented by a set of equality constraints which can be mathematically represented as follows:

$$J = \sum_{i=1} e_i^2 \quad (15)$$

$$C_j = \ddot{q}_j^* - \ddot{q}_j \quad \forall j \quad (16)$$

210 where e_i is the control input/excitation of i^{th} actuator at time t and q_j is the j^{th} generalized coordinate.
 211 Since for many \ddot{q}_j^* the muscles might not be able to produce sufficient forces, usually ideal torque actuators
 212 are added to the musculoskeletal model to prevent the fast target formulation from failing. Usually, the
 213 forces/torques produced per unit control effort for the ideal actuators is much lower than muscles. In
 214 such setups, following equation 15, ideal torque actuators produce significant force/torque only when the
 215 muscles are saturated, and hence they are also referred to as reserve actuators. Since the CMC tool does not
 216 support event detection based disabling of constraints, the seat contact force was supplied as an external
 217 force rather than a kinematic constraint. The seat force was pre-computed for the target STS trajectory
 218 before running the CMC tool.

4 RESULTS

219 We increased strength deficits in steps of 20%, and generated STS trajectories for each model. The
 220 optimization was performed three times for each model, and this study reports the trajectory with the
 221 lowest cost (Equation 2) among them. The optimization could generate successful STS trajectories for the
 222 0%, 20%, and 40% strength deficit models. However, for the 60% strength deficit model, the optimization
 223 framework could only generate a successful STS trajectory when the model was assisted externally at the
 224 torso. For conciseness, we refer to these trajectories as those of the models even though the models were
 225 only one component of the complete optimization framework.

226 The STS motion is divided into four phases as suggested in Millington et al. (1992) to facilitate discussions.
 227 Figure 4 shows these four kinematics-based phases for the STS trajectory of the 0% strength deficit model.
 228 Phase 1 starts with the trunk flexion and ends when the knee extension starts. Phase 2 starts with the knee
 229 extension and ends when the hip joint is maximally flexed. Phase 3 begins with the reversal of trunk flexion
 230 to extension and ends with the model standing upright. Mathematically the end of phase 3 is defined as the
 231 time when the horizontal velocity of the COM becomes zero. Phase 4 is the balancing phase, and during it,
 232 the model sways back and forth while standing. We have not any observations about the features of phase 4

233 in this study as the STS transition is complete at the end of phase 3. The dotted black lines in Figures 4-6
234 marks the transition between the four phases.

235 The results are organized into three subsections. In subsection 4.1 first, the common patterns among the
236 unaided STS trajectories are reported and contrasted against experimental observation of (Caruthers et al.,
237 2016). Then, the adaptations caused by muscle strength deficits are reported. Subsequently, in subsection
238 4.2, an explanation for the failure of optimization to generate STS using the 60% strength deficit model
239 is proposed. Finally, in subsection 4.3, the features of the STS trajectory generated using the externally
240 assisted 60% strength deficit model are discussed. Please refer to Figures 4-6 and Table 4 during the
241 following subsections for details.

242 **4.1 Unaided STS Transitions**

243 For all the unaided trajectories, the STS transition is initiated by activating the ILPSO muscle. ILPSO
244 activation generates torque around the hip joint and flexes the torso forward. It is followed by the
245 deactivation of ILPSO muscle and gradually increasing activations of the GMAX and HAMS muscles. The
246 GMAX and HAMS muscles undergo eccentric contraction to control the torso's forward flexion. As the
247 end of Phase 1 approaches, the activation of VAS muscle is increased to prepare for seat-off. Phase 1 ends
248 when the VAS muscle has generated sufficient torques around the knee joint to lift the musculoskeletal
249 model off the chair. During phase 2, the activation of GMAX, HAMS, and VAS muscles continues to
250 increase. The GMAX and HAMS activation reduces the hip flexion velocity until it becomes zero. At this
251 point, the trunk is maximally flexed, phase 2 comes to an end. The knee joint extends only slightly during
252 phase 2. During phase 3, the activation of GMAX, HAMS, and VAS muscles first increases, then peaks,
253 and finally tapers off. These patterns lead to the extension of both the hip and knee joints until the standing
254 posture is achieved. The tapering off of the GMAX, HAMS, and VAS muscle activations during the latter
255 half of phase 3 occurs because smaller forces are required to continue standing up since an increasing
256 fraction of body weight is borne by bone alignment. At the end of phase 3, both the ILPSO and GAS are
257 activated to stop the hip and knee joints from extending past the upright posture. Significant TA muscle
258 activations are present during phase 1, phase 2, and the first half of phase 3. These activations produce
259 the force needed to balance the counteracting SOL and GAS muscle forces. The SOL and RF muscles
260 see almost negligible activation throughout the three phases. During phase 3, as the ankle plantarflexes,
261 the passive fiber forces of the SOL muscle reduce. The peak GMAX, HAMS, and VAS muscle forces, as
262 well as the peak hip and knee extension torques, occur during the first half of phase 3 (Figure 6). As the
263 moment arms for muscles change with joint angles (Sherman et al., 2013), the peak forces and the peak
264 contributions to net joint torques usually do not coincide (Figure 6). For example, during phase 3, the VAS
265 muscle's peak contribution to net knee torque occurs later than the peak force. Because of the increased
266 moment arm, the VAS muscle is able to generate peak contribution to net joint torque with reduced muscle
267 force.

268 The general activation patterns of GMAX, HAMS, VAS, SOL, and TA muscles match those
269 experimentally observed in Caruthers et al. (2016); however, those of RF and GAS muscles do not.
270 Caruthers et al. (2016) reports significant activations of RF muscle from phase 1 through the first half of
271 phase 3, while our trajectories feature only minimal activation of RF muscle during the same. Our STS
272 trajectories feature a GAS muscle activation during the latter half of phase 3, while Caruthers et al. (2016)
273 reports no such peak. Our trajectories feature significant activation of VAS muscle during the first half
274 of phase 1, while Caruthers et al. (2016) reports minimal activation during the same time. Although it is
275 difficult to comment on these discrepancies because of the nonlinear non-convex nature of optimization, the

276 cost terms C_3 and C_7 are most likely responsible for the VAS and RF muscle discrepancies, respectively.
277 Caruthers et al. (2016) does not report activations for ILPSO muscle.

278 The activation patterns of VAS, GMAX, HAMS and SOL muscles observed in this study are similar to
279 those of STS trajectories generated in Pandy et al. (1995), and Bobbert et al. (2016). The GAS muscle
280 activation patterns between this and Pandy et al. (1995) are also similar while Bobbert et al. (2016) does
281 not report the same. Pandy et al. (1995) observes significant RF activation throughout the STS transition,
282 Bobbert et al. (2016) observes it only before seat-off while our STS trajectories feature negligible RF
283 activation throughout STS transition. The variation TA muscle activation patterns between the three studies
284 were most like because of the assumption of initial sitting posture. The musculoskeletal model of Pandy
285 et al. (1995) does not contain ILPSO muscle while Bobbert et al. (2016) does not report ILPSO activations.

286 With strength deficits, the STS duration increases, while the peak COM vertical velocity, peak GMAX,
287 and VAS muscle forces and their respective contributions to peak net joint torques decrease (Table 4, Figure
288 6). With increasing strength deficits, the VAS muscle starts getting saturated first, followed by the GMAX
289 muscles. When the VAS muscle is not saturated, the HAMS muscle works with the GMAX muscle to
290 control hip extension. When the VAS muscle starts getting saturated, the activation of HAMS muscle is
291 reduced as it works opposite to VAS muscle along the knee joint. The reduced activation of HAMS muscle
292 increases the stress on the GMAX muscle. The contribution of HAMS muscle to the peak net knee joint
293 torques drops from -22.80% , -27.94% for the 0% and 20% strength deficit models to -12.91% for the
294 40% strength deficit model. While, the contribution of HAMS muscle to the peak net hip joint torques
295 drops from 49.17% , -49.48% for the 0% and 20% strength deficit models to 37.14% for the 40% strength
296 deficit model. The contribution of GMAX to peak net hip joint torques increase from 54.46% , 54.22%
297 for the 0% and 20% strength deficit models to 64.58% for the 40% strength deficit model. Bobbert et al.
298 (2016) also observes, reduced explosiveness in STS with increased strength deficits. However, Bobbert
299 et al. (2016) does not observe a significant reduction in HAMS muscle activation. This difference exists
300 most likely because Bobbert et al. (2016) used the solution of the previous optimal trajectory as the initial
301 for the next optimization problem.

302 4.2 Failure to produce STS transition

303 The optimization framework failed to generate the STS transition for the 60% strength deficit model. We
304 suspected the GMAX or the VAS muscle to be responsible for this failure as they were getting saturated
305 during the STS trajectory of the 40% strength deficit model (Figure 6). The TA muscle was also getting
306 saturated; however, we did not inspect it since the TA muscle can easily be relieved by moving the feet
307 slightly forward. Moving the feet slightly forward will reduce the amount of ankle dorsiflexion and the
308 accompanying passive fiber forces of the counteracting SOL muscle.

309 We used the 60% strength deficit model and OpenSim CMC Tool to track the successful STS motion of
310 40Two different setups of reserve actuators were used to aid the muscles. In the first setup, the optimal
311 torque, i.e., torques generated per unit control effort, for the hip and knee torque actuators were 100Nm
312 and 1Nm respectively, while in the second setup, they were 1Nm and 100Nm . The first setup favored
313 the utilization of the hip reserve actuator, while the second setup favored the utilization of the knee
314 reserve actuator. The motion-tracked using the first setup features a peak torque of -38.64Nm by the
315 knee reserve actuator and increased activation of both VAS and RF muscles. While the second setup-based
316 motion-tracking features a peak torque of only -3.66Nm by the hip reserve actuator and increased HAMS
317 and GMAX activations. The lower magnitude of reserve actuator in the second setup compared to the first
318 supports the hypothesis that the failure to generate STS motion for the 60% strength deficit model was

319 because of VAS muscle weakness. Also, the HAMS was not saturated during the STS motion of the 40%
320 strength deficit model (Figure 6) and could be actuated to assist GMAX if needed, further supporting the
321 hypothesis. Also, the magnitude of reserve actuators shows that it is possible to assist the model only at the
322 knee joint for successful STS transition without significant modification of motion.

323 **4.3 Externally assisted STS transition**

324 It was observed in the last subsection that assisting the musculoskeletal model primarily at the hip joint
325 leads to increased RF muscle activation while assisting it primarily at the knee joint leads to increased
326 HAMS muscle activation. As STS transition is performed several times a day, assisting only at the hip or
327 the knee joint will lead to the contracture of the RF or the HAMS muscle, respectively. As both the muscles
328 cross the hip joint in an antagonistic manner, their contracture has a high potential to lead to back pain
329 issues. Thus the external assistance was introduced at the torso COM in the 60% strength deficit model.
330 Also, assisting the model at the torso center of mass is a good approximation for assisting a human at the
331 underarms area. The underarms area is easily graspable, and assistance using it helps simplify the design of
332 a probable STS assistance device.

333 Physical assistance, when provided in an assist-as-needed manner, can help maintain or recover lower
334 extremity strength. Thus while generating the assisted STS trajectories, the over-utilization of external
335 assistance was penalized (Equation 8). Figure 5 shows the body postures and the assistance force trajectories
336 from the STS motion generated using the externally assisted 60% strength deficit model. The STS trajectory
337 features utilization of external assistance only when the VAS muscle starts getting saturated, i.e., it uses
338 external assistance only when needed. The peak magnitudes of the vertical and horizontal components of
339 external assistance are 323.81N and 77.53N , respectively. The external assistance is used to assist muscles
340 at both the hip and knee joints, as evidenced by the reduced peak net hip and knee joint torques (Table 4).
341 The peak VAS, GMAX, and HAMS muscle forces are also lower than those from the STS motion of 40%
342 strength deficit models (Figure 6).

5 CONCLUSION

343 This publication presented and analyzed the STS trajectories generated using open-loop single shooting
344 optimization for musculoskeletal models with different muscle strength deficit levels. The strength deficits
345 were introduced by scaling the maximum isometric strength of all the muscles in steps of 20%. The strength deficits
346 could successfully generate STS trajectories for 0%, 20%, and 40% strength deficit models. As
347 muscle strength deficit increased, the peak VAS and GMAX forces, peak center of mass velocities reduced
348 while the STS increased. When the VAS muscle started getting saturated (40% strength deficit model),
349 the activation of the antagonistic HAMS muscle was reduced. The reduced HAMS muscle activation led
350 to increased GMAX muscle activation. Then the motion-tracking results were used to propose the VAS
351 muscle weakness as the reason for optimization's failure to generate an STS trajectory using the 60%
352 strength deficit model. The motion tracking results were also used to motivate the introduction of external
353 assistance at torso COM. Optimization was able to generate a successful STS trajectory for the externally
354 assisted 60% strength deficit model. The trajectory featured lower peak GMAX, VAS, and HAMS muscle
355 forces and the usage of external assistance in an assist-as-needed manner. We hope the results will help
356 plan interventions and design novel STS assistance devices and thus have made all the source material
357 public. However, the findings of this study should be observed with caution as it they have many inherent
358 assumptions. The most significant among these known assumptions are discussed in the next paragraph.

359 Strength deficits were introduced by scaling the maximum isometric strength of all the muscles
360 simultaneously. Bobbert et al. (2016) and Yokota et al. (2016) also introduced strength deficits in a

similar manner. However, it might be the case that the strength of all muscles does not deteriorate by the same factor. Also, scaling the maximum isometric forces is not the only way to introduce strength deficits. For example, the peak muscle activations could have been limited to the same effect. Many studies have experimentally reported that the elderly flex their trunk much more than healthy young adults. Thus the elimination of lumbar joint, even though also made by Pandy et al. (1995), Bobbert et al. (2016), and Yokota et al. (2016), might be an oversimplification. During simulation, the model could not adjust its feet relative to the chair. It might have prevented the discovery of less demanding trajectories. Other musculoskeletal model-related critical assumptions are the sagittal plane of symmetry and simplification of muscle groups to single musculotendon units. No control level coupling between muscles was implemented, i.e., the muscles could be activated or deactivated independently; however, such might not be the case. The cost function used in this study is not unique in its capability to engender STS. Further, even for the selected cost function, the relative weights of the different cost terms should have been chosen using inverse optimal control. The relative weights were heuristically selected because of the computationally demanding nature of the optimization. The generated STS trajectories are local optimal solutions of nonlinear non-convex optimizations. The optimization's failure to generate STS using the 60% strength deficit model might have been because of the optimization setup rather than muscle saturation.

In the future, we plan to use the results of this study to design a kinematic events-based closed-loop controller for STS transition. We also plan to conduct experiments against whom the musculoskeletal model simplifications, and the generated STS trajectories can be verified. Finally, we intend to design an STS assistance device that operates on the assist-as-needed principle.

6 AUTHOR CONTRIBUTIONS

7 DATA AVAILABILITY STATEMENT

The optimization source code and the results from this study are available <https://github.com/ShibataLab/STS>.

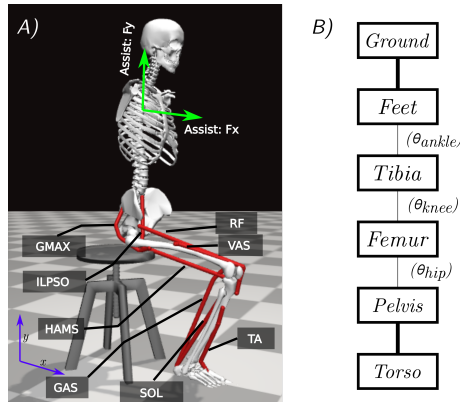


Figure 1. (A) The planar musculoskeletal model used for this study. The green arrows represent the horizontal and vertical component of external assistance force. (B) Degrees of freedom within the musculoskeletal model. Thick dark lines represent a weld joint.

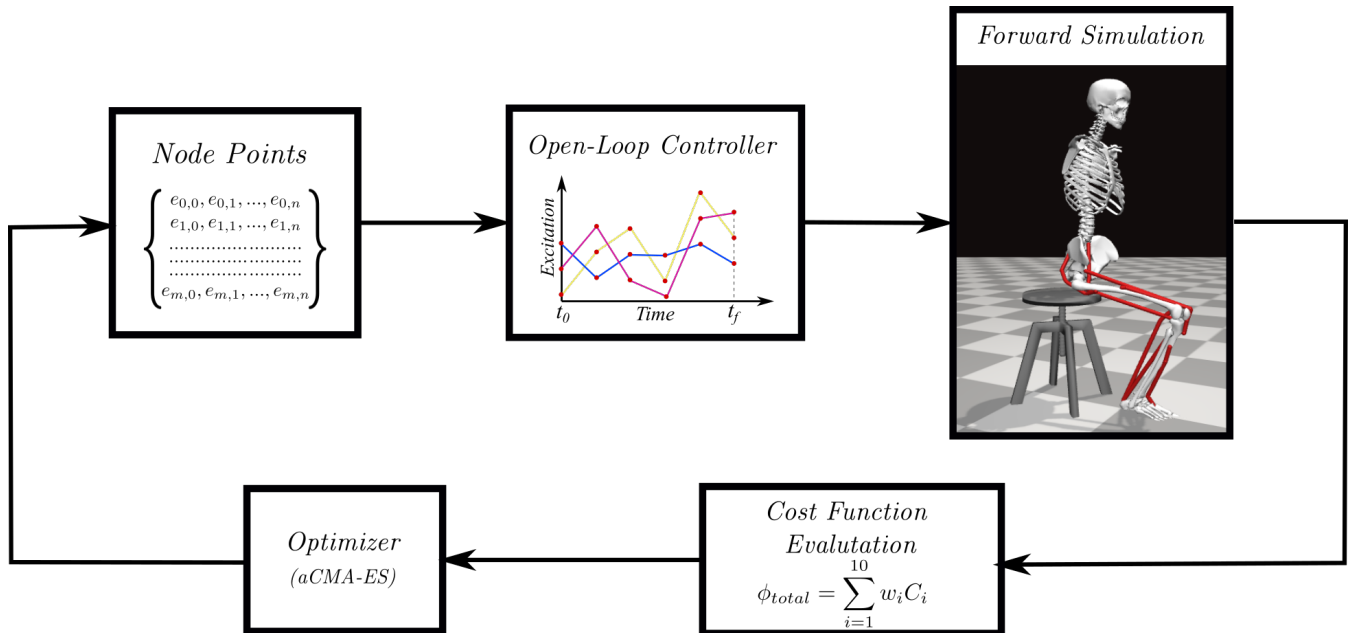


Figure 2. Overview of single shooting optimization framework. The red dots in the open-loop controller represents the node points obtained from the discretization of excitation trajectories.

Muscle	Acronym	Maximum Isometric Strength (N)
Vastus	VAS	19187.90
Gluteus maximus	GMAX	6675.17
Hamstrings	HAMS	8210.93
Iliopsoas	ILPSO	5394.69
Rectus Femoris	RF	4383.48
Gastrocnemius	GAS	9381.15
Soleus	SOL	15849.99
Tibialis Anterior	TA	4233.64

Table 1. Muscles included in the model, their acronyms and their respective maximum isometric strengths (0% strength deficit).

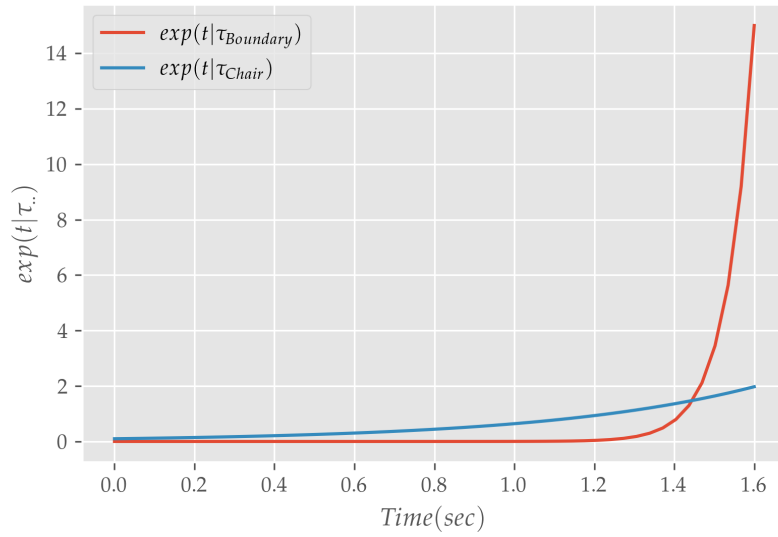


Figure 3. $\exp(t|\tau_{..})$ for $\tau_{Boundary}$, τ_{Chair} and $t_f = 1.6\text{sec}$

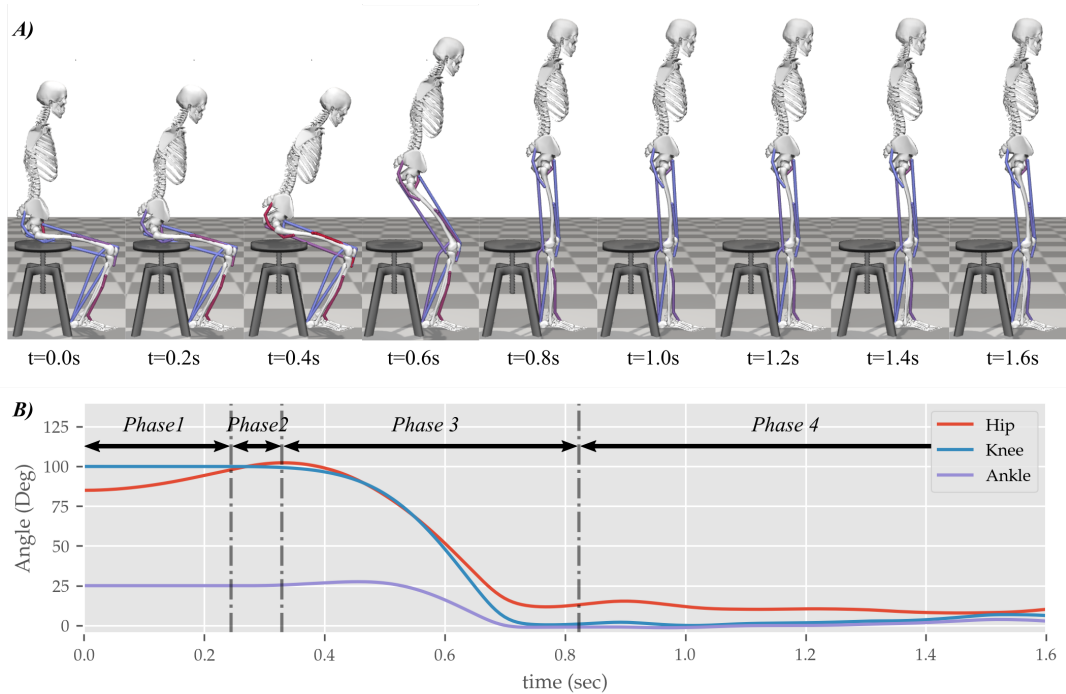


Figure 4. Postures (A) and joint angle trajectories (B) from the STS transition of 0% strength deficit model. In (A) the color gradient from blue to dark red represents the amount of muscle activation.

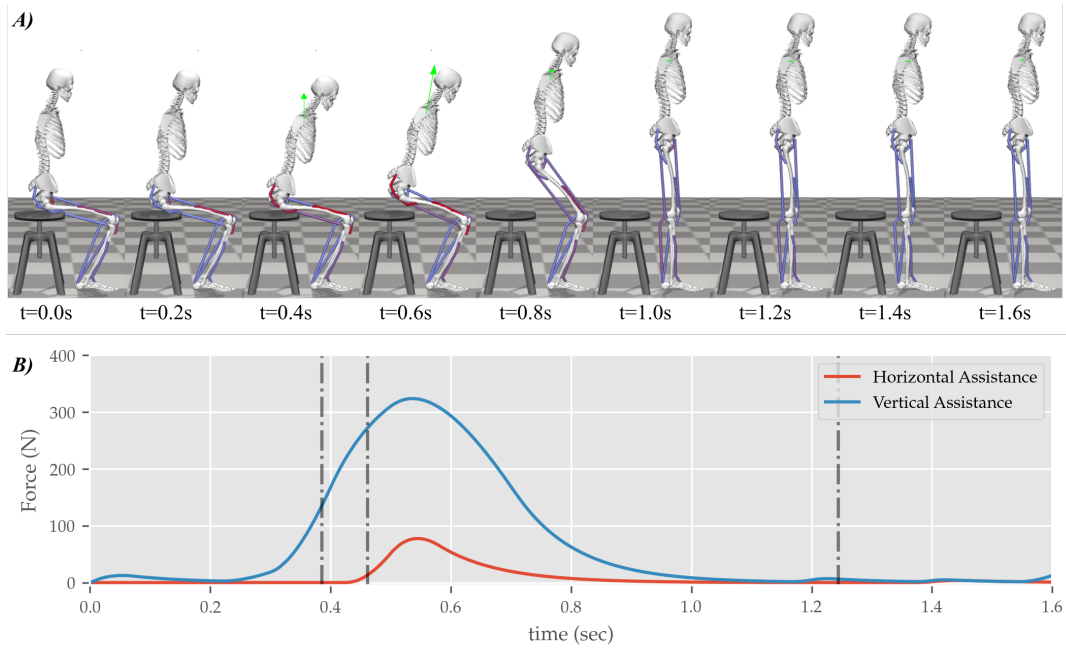


Figure 5. Postures (A) and the external assistance trajectories (B) from the STS transition of the externally assisted 60% strength deficit model. The green arrow in (A) represents the resultant external assistance force.

Table 2. List of Symbols

Variable	Description
t	time
t_0	Start Time
t_f	Final Time
θ_j	Angle of joint j
$..(t)$	Value of a expression .. at time t
$.. $	The absolute value expression ..
τ	time constant for $\exp()$ function
y_{com}	y coordinate of COM
x_{com}	x coordinate of COM
x_{talus}	x coordinate of ankle
$F_{m,n}$	component of contact force acting on body m in direction n
a_m	activation of muscle m
\dot{a}_m	rate of change of activation of muscle m
$\ F_{Assist}\ $	Magnitude of external assistance
$bool()$	boolean operation
$T_{n,limit}$	Torque generated by the torsional limit spring at the n^{th} joint
ZMP_x	Horizontal component of feet force ZMP

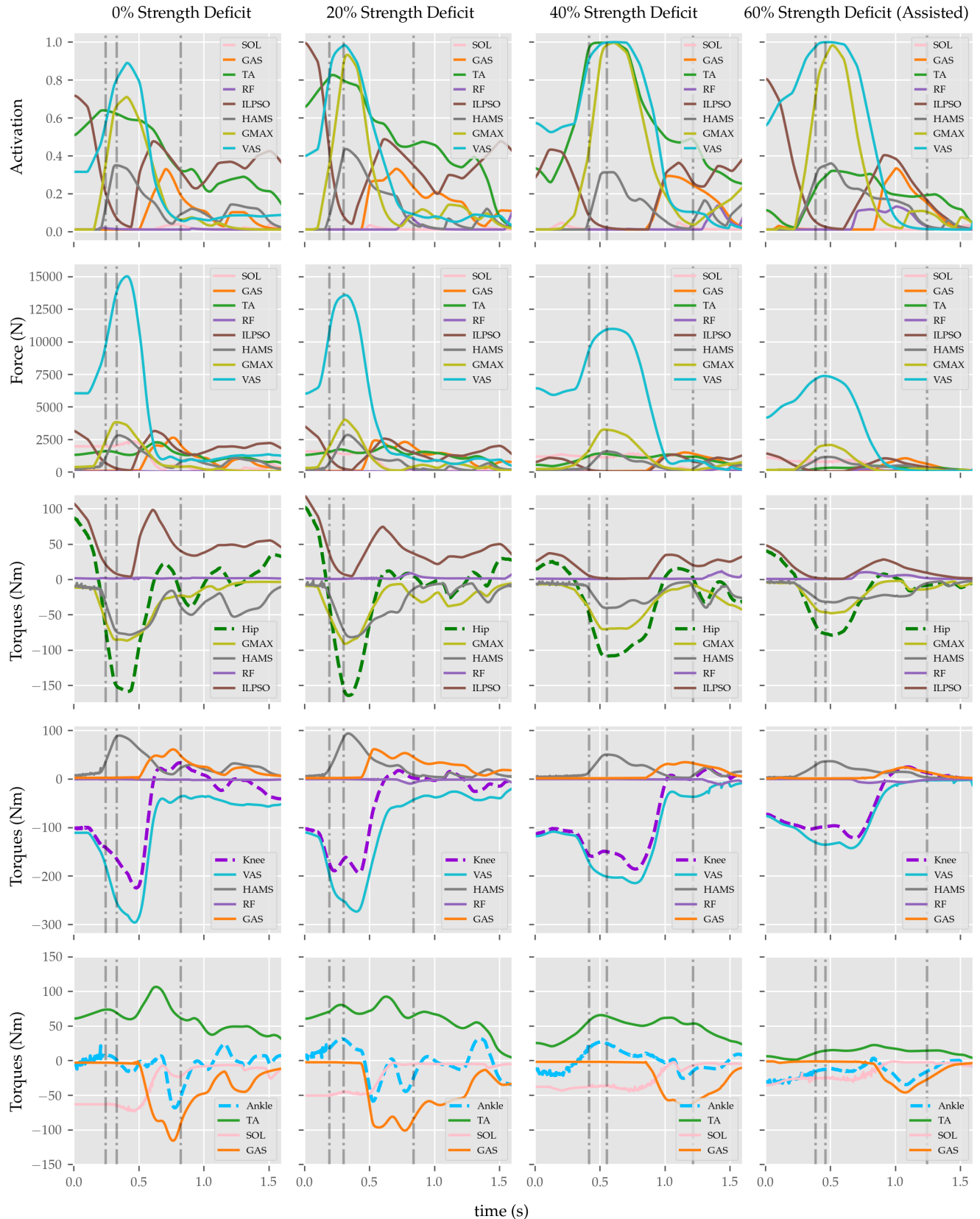


Figure 6. Muscle activations, muscle forces, and their contributions to the net hip, knee, and ankle joint torques from the STS trajectories of 0%, 20%, 40% and externally assisted 60% strength deficit models. The net joint torques are the torques required to reproduce the motion in the absence of all muscle actuators.

Table 3. List of hyperparameter values

Variable	Value
t_0	0sec
dt	0.1sec
$\tau_{boundary}$	$t_f/24$
τ_{chair}	$t_f/3$
w_1	800
w_2	600
w_3	0.4
w_4	100
w_5	20
w_6	0.2
w_7	10
w_8	0.1
w_9	20
w_{10}	0.1

Table 4. Properties from STS trajectories of the 0%, 20%, 40% and externally assisted 60% strength deficit models. The second row shows the time difference between peak knee and peak hip torques. Rows 5, 6, 8 and 9 shows contributions of muscles to peak joint torques.

# Row	Property	0% Strength Deficit	20% Strength Deficit	40% Strength Deficit	Externally Assisted 60% Strength Deficit
1	STS duration (s)	0.82	0.84	1.22	1.24
2	Peak COM Vertical Velocity (m/s)	1.25	1.04	0.93	0.85
3	Peak Hip Torque (Nm)	-158.77	-164.32	-108.86	-79.06
4	GMAX Peak Hip Torque (Nm)	-86.46	-89.10	-70.30	-47.92
5	HAMS Peak Hip Torque (Nm)	-78.06	-81.30	-40.43	-32.51
6	Peak Knee Torque (Nm)	-224.96	-193.59	-186.01	-121.86
7	VAS Peak Knee Torque (Nm)	-294.04	-271.14	-214.99	-140.15
8	HAMS Peak Knee Torque (Nm)	67.03	75.76	27.75	20.51
9	Peak VAS Force (N)	15024.52	13573.82	10988.08	7372.93
10	Peak GMAX Force (N)	3826.64	4005.31	3256.65	2072.87
11	Peak HAMS Force (N)	2808.96	2842.76	1572.41	1150.42

REFERENCES

- 383 Arnold, D. V. and Hansen, N. (2010). Active covariance matrix adaptation for the (1+ 1)-cma-es. In
384 *Proceedings of the 12th annual conference on Genetic and evolutionary computation*. 385–392
- 385 Bobbert, M. F., Kistemaker, D. A., Vaz, M. A., and Ackermann, M. (2016). Searching for strategies to
386 reduce the mechanical demands of the sit-to-stand task with a muscle-actuated optimal control model.
387 *Clinical Biomechanics* 37, 83–90
- 388 Caruthers, E. J., Schneider, G., Schmitt, L. C., Chaudhari, A. M., and Siston, R. A. (2020). What are the
389 effects of simulated muscle weakness on the sit-to-stand transfer? *Computer Methods in Biomechanics*
390 and *Biomedical Engineering* 23, 765–772
- 391 Caruthers, E. J., Thompson, J. A., Chaudhari, A. M., Schmitt, L. C., Best, T. M., Saul, K. R., et al. (2016).
392 Muscle forces and their contributions to vertical and horizontal acceleration of the center of mass during
393 sit-to-stand transfer in young, healthy adults. *Journal of applied biomechanics* 32, 487–503
- 394 [Dataset] CMA-ES (2013). libcmaes. <https://github.com/CMA-ES/libcmaes>
- 395 Delp, S. L., Anderson, F. C., Arnold, A. S., Loan, P., Habib, A., John, C. T., et al. (2007). Opensim:
396 open-source software to create and analyze dynamic simulations of movement. *IEEE transactions on*
397 *biomedical engineering* 54, 1940–1950
- 398 Geravand, M., Korondi, P. Z., Werner, C., Hauer, K., and Peer, A. (2017). Human sit-to-stand transfer
399 modeling towards intuitive and biologically-inspired robot assistance. *Autonomous Robots* 41, 575–592
- 400 Gross, M., Stevenson, P., Charette, S., Pyka, G., and Marcus, R. (1998). Effect of muscle strength and
401 movement speed on the biomechanics of rising from a chair in healthy elderly and young women. *Gait*
402 & *posture* 8, 175–185
- 403 Hughes, M. A., Myers, B. S., and Schenkman, M. L. (1996). The role of strength in rising from a chair in
404 the functionally impaired elderly. *Journal of biomechanics* 29, 1509–1513
- 405 Janssen, W. G., Bussmann, H. B., and Stam, H. J. (2002). Determinants of the sit-to-stand movement: a
406 review. *Physical therapy* 82, 866–879
- 407 Lai, A. K., Arnold, A. S., and Wakeling, J. M. (2017). Why are antagonist muscles co-activated in my
408 simulation? a musculoskeletal model for analysing human locomotor tasks. *Annals of biomedical*
409 *engineering* 45, 2762–2774
- 410 Lord, S. R., Murray, S. M., Chapman, K., Munro, B., and Tiedemann, A. (2002). Sit-to-stand performance
411 depends on sensation, speed, balance, and psychological status in addition to strength in older people.
412 *The Journals of Gerontology Series A: Biological Sciences and Medical Sciences* 57, M539–M543
- 413 Meijer, K., Willems, P. J., Savelberg, H. H., et al. (2009). Muscles limiting the sit-to-stand movement: an
414 experimental simulation of muscle weakness. *Gait & posture* 30, 110–114
- 415 [Dataset] Millard, M. (1999). First-order activation dynamics
- 416 Millington, P. J., Myklebust, B. M., and Shambes, G. M. (1992). Biomechanical analysis of the sit-to-stand
417 motion in elderly persons. *Archives of Physical Medicine and Rehabilitation* 73, 609–617
- 418 Mombaur, K. and Hoang, K.-L. H. (2017). How to best support sit to stand transfers of geriatric patients:
419 Motion optimization under external forces for the design of physical assistive devices. *Journal of*
420 *biomechanics* 58, 131–138
- 421 Ong, C. F., Geijtenbeek, T., Hicks, J. L., and Delp, S. L. (2019). Predicting gait adaptations due to ankle
422 plantarflexor muscle weakness and contracture using physics-based musculoskeletal simulations. *PLoS*
423 *computational biology* 15, e1006993
- 424 Pandy, M., Garner, B., and Anderson, F. (1995). Optimal control of non-ballistic muscular movements: a
425 constraint-based performance criterion for rising from a chair. *Journal of Biomechanical Engineering*
426 117, 15

- 427 Sadeghi, M., Andani, M. E., Bahrami, F., and Parnianpour, M. (2013). Trajectory of human movement
428 during sit to stand: a new modeling approach based on movement decomposition and multi-phase cost
429 function. *Experimental brain research* 229, 221–234
- 430 Schenkman, M., Hughes, M. A., Samsa, G., and Studenski, S. (1996). The relative importance of strength
431 and balance in chair rise by functionally impaired older individuals. *Journal of the American Geriatrics
432 Society* 44, 1441–1446
- 433 Sherman, M. A., Seth, A., and Delp, S. L. (2013). What is a moment arm? calculating muscle effectiveness
434 in biomechanical models using generalized coordinates. In *International Design Engineering Technical
435 Conferences and Computers and Information in Engineering Conference* (American Society of
436 Mechanical Engineers), vol. 55973, V07BT10A052
- 437 Thelen, D. G. and Anderson, F. C. (2006). Using computed muscle control to generate forward dynamic
438 simulations of human walking from experimental data. *Journal of biomechanics* 39, 1107–1115
- 439 Yokota, H., Ohshima, S., and Mizuno, N. (2016). Sit-to-stand motion analysis using multiobjective
440 genetic algorithm based on musculoskeletal model simulation. *IEEJ Journal of Industry Applications* 5,
441 236–244
- 442 Yoshioka, S., Nagano, A., Himeno, R., and Fukashiro, S. (2007). Computation of the kinematics and the
443 minimum peak joint moments of sit-to-stand movements. *Biomedical engineering online* 6, 1–14